Neutron-scattering studies of the two magnetic correlation lengths in terbium

K. Hirota and G. Shirane
Brookhaven National Laboratory, Upton, New York 11973

P. M. Gehring and C. F. Majkrzak
National Institute of Standards and Technology, Gaithersburg, Maryland 20899
(Received 26 October 1993)

Extensive neutron-scattering experiments have been performed in order to characterized the nature of the two correlation lengths observed in Tb, a phenomenon common to Ho as well as $SrTiO_3$. In the vicinity of the transition temperature, each of those crystals exhibits an anomalous two-component q profile in the critical scattering; the usual broad peak and an unexpected additional narrow peak. In order to clarify the spatial origin of the narrow component, the $(0,0,\delta)$ magnetic satellite peak of Tb has been closely examined using a very narrow neutron beam realized by a high *spatial* resolution reflectometer at the National Institute of Standards and Technology, which can produce well-defined beam widths of 0.3 mm and less. The small scattering angle ($\theta \approx 1.35°$) and the narrow beam width result in an extraordinarily fine q and E resolution. As recently reported, we have confirmed that the intensity of the narrow component is enhanced near the edge of the crystal; it demonstrates that the major part is located within the near surface volume or "skin" of the crystal. A skin thickness of $\sim$0.2 mm full width at half maximum (FWHM) is obtained by fitting the results to a model scatterer distribution which convolutes the beam profile. In contrast to the case of the central peak observed in $SrTiO_3$, this unusual spatial distribution establishes the narrow component as a distinct entity in the critical fluctuations. We have shown that the narrow component possesses a different temperature dependence of δ from that of the broad one. Moreover, high E resolution scans show that the narrow component has a distinct energy width which is smaller than our resolution limit ($\sim$2 μeV FWHM), and that it is essentially temperature independent. We believe that this *quasistatic* character of the narrow component is the important key to understanding its physical origin.

I. INTRODUCTION

In 1986, Andrews[1] reported an unexpected two-component line shape observed in the x-ray-scattering measurements of the critical scattering associated with the structural phase transition in $SrTiO_3$. At a temperature close to the phase transition temperature T_c, the critical scattering was qualitatively changed by the appearance of a very narrow peak superimposed on the already present broad peak. This implies the existence of a second, and much larger, length scale just above T_c. This discovery is remarkable in view of our current understanding of critical phenomena, in which only one correlation length is needed to characterize the average size of the fluctuating regions above T_c. Intensive studies of $SrTiO_3$ have been done up to the present.[2–4] Very recently, Thurston *et al.*[5] performed high q resolution neutron-scattering measurements on Ho, just above the spiral transition temperature, which revealed a similar two-component line shape. Figure 1 shows typical examples of this two-component line shape as well as the temperature dependences of the two correlation lengths for both $SrTiO_3$ and Ho. The results of these two experiments suggest that the narrow component is probably a feature that is common to many if not all phase transitions in condensed matter systems. Indeed, the two-component line shape has been observed in $RbCaF_3$ (Ref. 6) and $KMnF_3$ (Ref. 7), both of which undergo the same structural transition as does $SrTiO_3$. Studies on other systems are also in progress.

Determining the spatial origin of the narrow component is a crucial step that is needed for an ultimate understanding of the presence of the two length scales in critical phenomena. It is, however, not easy to make such a determination. X rays, which probe crystal surfaces to depths of order several μm, cannot tell if the narrow component is present in the crystal bulk. On the other hand, neutrons can probe the bulk, but have not yet been able to separate surface and bulk contributions. This problem was recently solved by Gehring *et al.*[8] By translating a cube-shaped Tb crystal through a well-defined narrow neutron beam, it was possible to isolate thin slices of the Tb sample and thereby pinpoint the location of the narrow component. The BT7 reflectometer at the Neutron Beam Split-core Reactor (NBSR) at the National Institute of Standards and Technology (NIST) is ideally suited to this purpose.[9] This reflectometer can vary the incident horizontal beam width from zero to several mm with an accuracy of $\pm$0.01 mm using motorized slits. Using this technique, Gehring *et al.* established that the origin of the unexpected narrow component in Tb lies in the near-surface volume or "skin" of the Tb crystal. In this context, the meaning of skin is distinct from that of surface because the narrow component is spread over

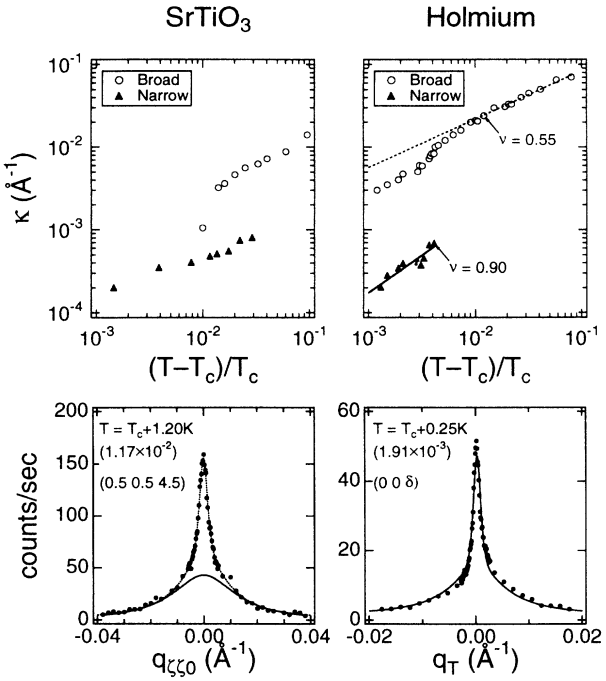

FIG. 1. Results of past studies on $SrTiO_3$ and Ho: Inverse correlation lengths of the narrow and broad components (top left), and a typical two-component line shape (bottom left) seen in x-ray scattering of $SrTiO_3$ (Ref. 3); inverse correlation lengths and fitting curves to a power law (top right), and a typical two-component line shape (bottom right) observed in high-q-resolution neutron scattering of Ho (Ref. 5).

several hundred micrometers and not just one or two.

We have performed a comprehensive study on a single crystal of Tb using a variety of neutron-scattering techniques. In comparison to other rare-earth metals such as Ho and Dy, Tb has a lower neutron absorption and a smaller spiral wave vector δ. Both of these properties are advantageous for the current study because of the need to use a narrow beam, which results in a reduced signal, and the need to work in the forward direction at very low scattering angle. Tb crystallizes in the hexagonal close-packed structure and has a measured saturation magnetic moment of $9.34\mu_B$/atom, which results from a $^7F_6$ ground state of eight electrons in the $4f$ shell. Tb exhibits a magnetically ordered spiral phase below $T_s \approx 230$ K.[10] Pairs of magnetic satellite peak appear around each nuclear Bragg peak offset by $(0, 0, \pm\delta)$, where δ is proportional to the spin turn angle per atomic plane. With decreasing temperature, δ decreases continuously without showing any lock-in behavior as seen in other rare-earth metals.[11] At $T_c \approx 220$ K, a transition takes place in which the spins align ferromagnetically in the basal plane and δ drops discontinuously to zero.

In this paper, we present the results of more detailed experiments on the spatial distribution of the narrow component, in addition to an overall picture of the critical scattering in Tb. We have estimated the spatial extent of the narrow component on the basis of a model calculation. We also show the energy scales for both broad and narrow components, which have been measured with very high E resolution. In contrast to the case of the central peak in $SrTiO_3$,[4] our experiments imply that the narrow component is a distinct entity that contributes to the scattering associated with the critical fluctuations above T_s. We believe that this *quasistatic* character of the narrow component is an important key which may resolve the physical origin of the second length scale. To this end, we conclude by discussing our results in the context of various theories which pertain to the two-length-scale problem.

II. EXPERIMENTAL DETAILS

The single crystal specimen of Tb used in this study was grown and prepared by B. Beaudry of the Materials Preparation Center at Ames Laboratory. The sample is a $7.1 \times 6.4 \times 7.1$ mm^3 cube with faces cut normal to the [1 0 0], [0 1 0], and [0 0 1] directions in an orthorhombic index with lattice constants $a = 6.273$ Å, $b = 3.601$ Å, and $c = 5.693$ Å at room temperature. The sample was polished on all sides with 0.5 μm alumina powder and electropolished in a mixture of methanol and perchloric acid. This procedure removes layers damaged by the cutting process and leaves behind a passive coating of one or two layers of an oxychloride of Tb that prevents subsequent oxidation of the Tb surface. This crystal was studied extensively by magnetic x-ray scattering[11] and has already been shown to be of high quality. The miscut of the [0 0 l] surface was determined directly with neutrons by measuring the mirror reflection from the Tb c-axis surface at the BT7 reflectometer. The resulting broad mirror reflection implies that the crystal surface does not have a perfect mirror finish. The reflection was, however, very sharply peaked at a position corresponding to a miscut of 0.25°. The crystal mosaic at $(0, 0, \delta)$ is very small; the half width at half maximum (HWHM) is only 0.17°.

The H8 triple-axis spectrometer located in the High Flux Beam Reactor at Brookhaven National Laboratory (BNL) was used for overall studies of the critical scattering of Tb. The H8 spectrometer was set up in a double-axis (no analyzer) mode and a standard triple-axis mode using incident neutron energies of 14.7 meV (wavelength $k_i = 2.67$ Å^{-1}) and 4 meV ($k_i = 1.39$ Å^{-1}) with a tight collimation 10′-10′-sample-10′-open and 10′-10′-sample-10′-10′. The $(0, 0, 2)$ reflection of pyrolytic graphite (PG) was used to monochromate the neutron beam, together with either a PG or Be filter to eliminate higher-order contamination from the incident beam.

Studies of the spatial origin of the second length scale in Tb were performed on the BT7 reflectometer in the NIST NBSR. As mentioned in the previous section, this reflectometer provides an incident horizontal beam width which can be varied from zero to several mm with an accuracy of ±0.01 mm using motorized slits positioned upstream from the sample. The BT7 reflectometer operates in a double-axis mode with a PG filter positioned before a vertically focused PG monochromator set at the $(0, 0, 2)$ reflection. The incident wave vector k_i is fixed at 2.35 Å^{-1}. The first slit (S1) sits 15 cm downstream

from the monochromator. The second one (S2) is 28 cm in front of the sample stage and 152 cm away from S1. The third slit (S3) is positioned in front of the detector. Although the long axis of these slits points vertically, they are referred to as horizontal divergent slits because they control the horizontal beam width and the divergence. Three different beam widths were used on the BT7 reflectometer. All were measured by translating a thin horizontal divergent slit (0.18 mm wide), fixed at the sample position, through the main beam, and then fitting the resulting line shape with a trapezoid function convoluted with the slit resolution. To avoid ambiguity, all widths hereafter refer to the full width at the bottom of the trapezoid obtained from the fitting.

In order to resolve both narrow and broad components of the critical scattering, it is necessary to have extremely good q resolution. Since the resolution width along the transverse direction becomes narrower for smaller scattering vectors, we have chosen a satellite peak at $(0,0,\delta)$, as already applied successfully to the measurements on Ho.[5] Figure 2 illustrates this dramatic change in transverse q resolution by comparing the scattering profiles of equivalent satellite peaks below T_s at $(0,0,\delta)$ and $(0,0,2+\delta)$ measured on H8. The transverse q width at $(0,0,\delta)$ has a HWHM of 0.0002 Å^{-1}, which is over 30 times smaller than the corresponding HWHM of 0.0065 Å^{-1} measured at $(0,0,2+\delta)$. These values are in excellent agreement with those expected from calculation of the resolution function.[12] In the same scattering geometry, the BT7 reflectometer can provide even better resolution. Using a beam width of 0.80 mm, the same transverse q scan yields a HWHM of only 0.000 03 Å^{-1}. As for longitudinal q scans at $(0,0,\delta)$, the measured HWHM is 0.0063 Å^{-1} at H8 and 0.0020 Å^{-1} at BT7. By comparison, the mosaic of 0.17° HWHM measured on BT7 at $(0,0,\delta)$ corresponds to 0.0004 Å^{-1}.

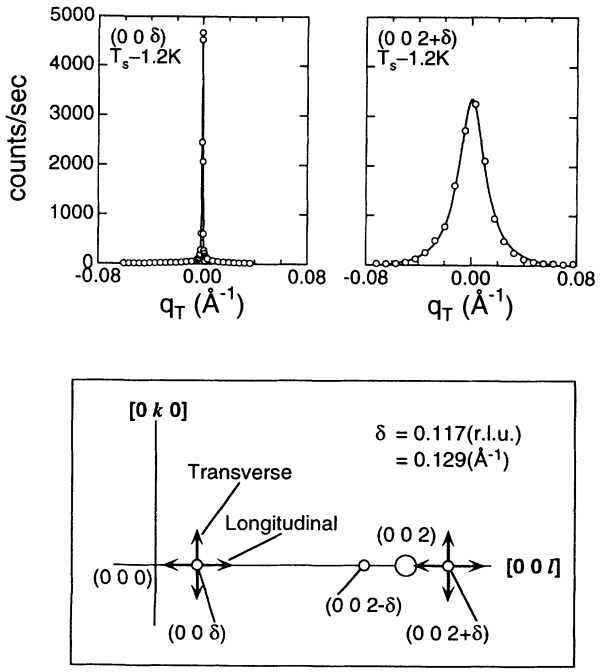

FIG. 2. (top) Transverse-q scans of equivalent satellite peaks below T_s at $(0,0,\delta)$ and $(0,0,2+\delta)$, measured on H8 in BNL using E_i = 14.7 meV and 10′-10′-S-10′-open; (bottom) schematic diagram of Tb reciprocal lattice.

III. PARAMAGNETIC TO MAGNETIC SPIRAL PHASE TRANSITION AT T_s

Figure 3 shows the inverse of the peak intensity in the longitudinal scan at $(0,0,\delta)$, the magnetic spiral wave

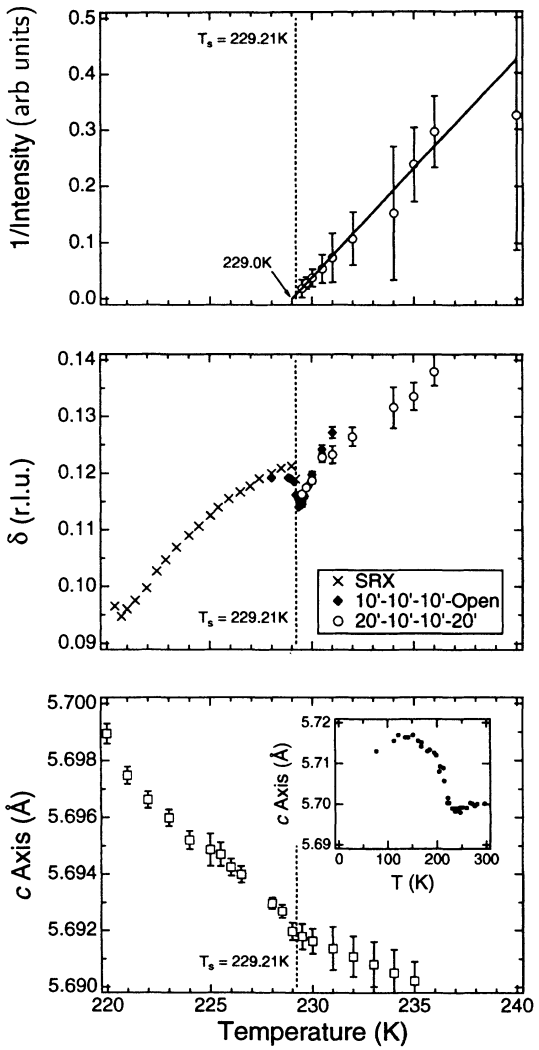

FIG. 3. Temperature dependence of basic parameters of Tb around the paramagnetic to magnetic spiral phase transition at T_s = 229.21 K, measure on H8 in BNL. (top) Inverse peak intensity in the longitudinal scan at $(0,0,\delta)$; (middle) spiral wave vector δ measured by x-ray (Ref. 11) and neutron scattering; (bottom) lattice constant along the c axis. The reported result (Ref. 13), taken over a wide temperature range, is shown in the inset.

vector δ, and the c-axis lattice constant as function of temperature. The peak intensity is obtained by fitting a Lorentzian to the data in the temperature range where neither the narrow component nor the Bragg peak is dominant. Thus, the figure essentially shows only the broad component. Note that the broad component does show near divergence at T_s: The inverse of the intensity is extrapolated to a very small but finite value at T_s. The extrapolated line becomes zero at 229.0 K, $\Delta T = 0.21$ K lower than $T_s = 229.21$ K. Heuristically, one can define a degree of first-order transition by the value of ΔT divided by the transition temperature. The $\Delta T/T_s$ in our case is about 10^3, which is much smaller than that of a typical magnetic first-order transition.

The lattice constant shows a continuous temperature dependence with no significant anomaly between 200 and 240 K, and becomes almost constant between 240 K and 260 K. This feature is consistent with the reported result,[13] taken over a wide temperature range, and is shown in the inset of Fig. 3. Due to a large magnetostriction, the c axis of Tb is elongated below T_s and has a broad peak around 150 K. However, there is no discontinuity in the lattice parameter at any temperature.

The temperature dependence of the intensity and the lattice constant indicate that the transition is very close to second order. However, the temperature dependence of δ shows a rather curious behavior. In addition to that reported in the resonant x-ray-scattering measurement,[11] we could observe a continuous change of δ in the region of the critical scattering up to 240 K, and found an anomaly near T_s, which is referred to as a sharp upturn in Refs. 8 and 11. With decreasing temperature, δ drops at a few kelvin above T_s, then starts increasing again in the temperature range where the narrow component appears. This sharp drop near T_s may cause difficulties in determining critical exponents. Another peculiarity is a very long relaxation of the intensity after changing temperature. It takes almost 30 min to saturate the intensity at 229.25 K after cooling from 230.0 K. Thus, we measured the intensity at each temperature after waiting a sufficient length of time to ensure the Tb sample had reached thermal equilibrium. Under these conditions, no thermal hysteresis is observed in the present measurements. The hysteresis effects previously reported[8,11] are presumably due to this relaxation.

Figure 4 shows the temperature dependence of the peak intensity at $(0,0,\delta)$, which shows a rapid change in intensity over a very narrow temperature range. Because of the sharpness of the transition and the long relaxation time involved, the thermal stability of the temperature controller is of crucial concern. We optimized our temperature control further to achieve a long time stability of less than ± 0.01 K with a thermal resolution of 0.02 K. Since the narrow component appears in a very limited temperature range and the order parameter changes very sharply, it is necessary to determine T_s very precisely. For that reason, we have utilized a unique advantage of neutron scattering and measured the temperature dependence of the scattered intensity at $(0,0,\delta)$ with the spectrometer set at several different, but very small, energy

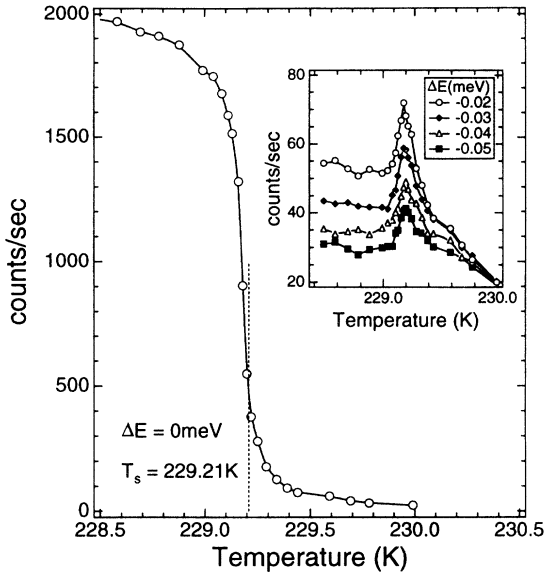

FIG. 4. Temperature dependence of the peak intensity at $(0,0,\delta)$, measured on H8 in BNL using $E_i = 14.7$ meV and 10′-10′-S-10′-10′. The inset shows the intensity derived from transverse scans at small energy transfers in the vicinity of T_s.

transfers. This trick exploits the extremely good E resolution available at small scattering angle, thereby eliminating a large fraction of the elastic scattering from the total scattering. The temperature dependence of the critical scattering so obtained exhibits a peak which shifts very slightly to lower temperature the lower the energy transfer. The value of T_s is determined by extrapolating the peak position to zero energy transfer. The inset of Fig. 4 shows a distinct peak at 229.21 K, which we defined as the transition temperature T_s to the spiral phase.

Our preliminary measurements indicate that the transition at T_s is very close to second order, despite the sharpness of the transition. Note that the sharpness does not necessarily imply a first-order transition, as is well known because of the intensive studies on KDP (KH_2PO_4),[14] in which a pure second-order shows a discontinuity in the temperature dependence of the order parameter. In the following sections, the measurements were mainly performed in a very small temperature range around T_s. All the measurements have been carried out after carefully waiting for thermal equilibration. In addition, the strong temperature dependence of δ required realigning the crystal after each temperature change.

IV. TWO-COMPONENT q PROFILES AT $(0,0,\delta)$

Longitudinal and transverse q scans at $(0,0,\delta)$ obtained at the H8 spectrometer are presented in Fig. 5 for three typical temperatures. The crystal was first heated to temperature well above T_s, then subsequently cooled down. The bottom figures show critical scattering well

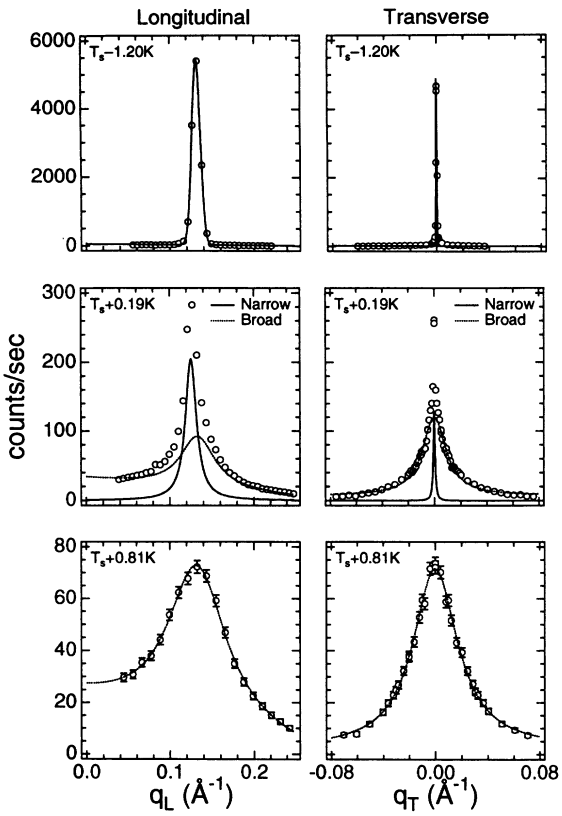

FIG. 5. Longitudinal- (left) and transverse- (right) q scans at $(0,0,\delta)$ obtained on H8 in BNL using $E_i = 14.7$ meV and 10′-10′-S-10′-open. Solid and dotted curves represent fits to a Lorentzian-squared and a Lorentzian line shape, convoluted with the resolution. These correspond to the narrow (or Bragg) component and the broad component, respectively.

above T_s, which exhibit only a broad peak. The broad critical scattering can be seen at as much as 10 K above T_s. With decreasing temperature, the peak becomes narrower and more intense. At temperatures very close to T_s, the line shape is modified by the appearance of a second, very narrow peak. The middle panels show the two-component line shape in the critical scattering. The narrow component begins to appear at about $T_s + 0.6$ K in the transverse scan. In spite of relatively broader longitudinal resolution, the two-component line shape is still visible below $T_s + 0.4$ K in longitudinal scans. Note that the peak positions of the narrow and broad components appear slightly shifted from each other in the longitudinal scans. This implies that the temperature dependence of the wave vector δ is not the same for each component. As shown in Fig. 6, the narrow component initially appears at a smaller δ than does the broad component, but then shifts to a larger δ with decreasing temperature. Two peak positions finally merge near T_s. The top row shows scans taken well below T_s, which illustrates the resolution limits for the respective experimental conditions noted in the preceding section.

The curves in the middle and bottom panels of Fig. 5 represent fitting curves to a Lorentzian-squared (for the

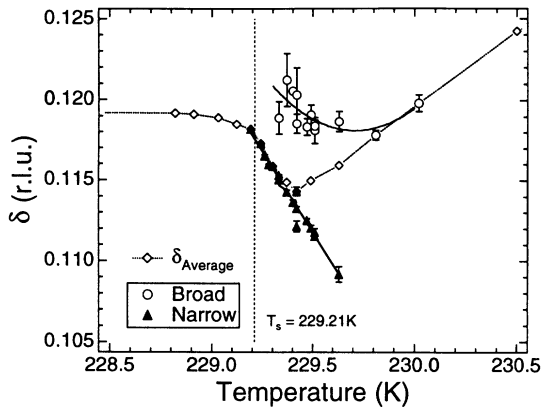

FIG. 6. Temperature dependence of the wave vectors δ for the broad and narrow components. The dotted curve represents δ obtained by fitting data with a single Lorentzian.

narrow component) and a Lorentzian (for the broad one) line shape convoluted with an appropriate resolution function. This combination of line shapes gives slightly better results on the whole than the others. Furthermore, this is eventually consistent with previous work on two length scale phenomena in other materials.[3,5]

The inverse correlation lengths of the broad and narrow components (κ_B and κ_N), i.e., the HWHM of the Lorentzian and $\sqrt{\sqrt{2}-1}$ times the HWHM of the Lorentzian-squared line shape, are plotted against the reduced temperature $t = (T - T_s)/T_s$ in Fig. 7. The

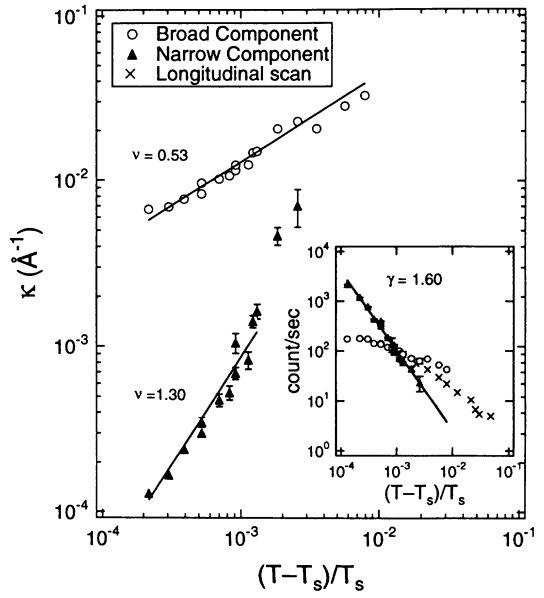

FIG. 7. Inverse correlation lengths of the narrow and broad components derived from transverse-q scans, associated with lines representing fits to a power law. Peak intensities of both components in transverse-q scans and those of longitudinal scans are plotted in the inset. These data were obtained on H8 in BNL using $E_i = 14.7$ meV and 10′-10′-S-10′-open.

peak intensities for both components are also presented in the inset of Fig. 7. The inverse correlation lengths of both components exhibit power law behavior in the observed temperature range and differ by a factor of 10 in magnitude. It is certain that the intensity of the narrow component does diverge at T_s as shown in the figure. However, the broad component probably stays finite in both intensity and width. This result is consistent with the preliminary result of the longitudinal scan shown in Fig. 3. Moreover, the intensity of the broad component obtained in the transverse scans is in good agreement with that obtained in the longitudinal scans. Comparing with the results of Ho and $SrTiO_3$, the widths of the broad and narrow components have similar properties in magnitude of the length scale and temperature dependence. (See Fig. 1.)

V. ENHANCEMENT OF THE NARROW COMPONENT IN THE SKIN

In order to study the spatial distribution of the narrow component, we measured the intensity of the $(0, 0, \delta)$ satellite peak while translating the crystal through a very narrow beam on the BT7 reflectometer. The scattering geometry is shown schematically in Fig. 8(a). The Tb crystal was mounted with the [1 0 0] axis vertical. The [0 0 1] direction was aligned along the translation axis of a motorized goniometer stage so that the narrow neutron beam could selectively probe thin slices of the Tb crystal, as depicted by the shaded area. The translation scale was set so that zero corresponds to the front face of the crystal. It should be emphasized that this capability requires the incident beam to be essentially parallel to the crystal surface, as is the case when working in the forward direction. Moreover, as we discuss later, any slight misorientation of the sample in either scattering angle θ or tilt angle has a significant effect on the estimate of the skin thickness. Therefore, the sample must be aligned very carefully.

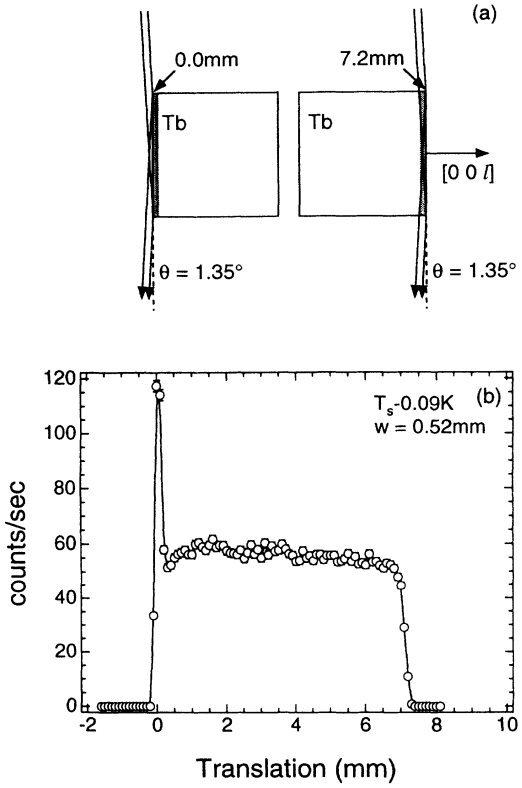

FIG. 8. (a) Schematic diagram of scattering geometry. (b) Translation scans at $(0, 0, \delta)$ below T_s at beam width at the base of 0.52 mm measured on BT7 in NIST.

A typical translation scan below T_s for the beam width of 0.52 mm is shown in Fig. 8(b). The intensity is greatly enhanced at the front edge compared to the rest of the crystal, because there effects due to absorption and extinction are minimal. Since both absorption and extinction are constant in the crystal bulk, the peak intensity also remains constant. Eventually, the peak intensity drops to zero as the crystal moves out of the beam at the back edge. In order to avoid having to correct our scans for both absorption and extinction effects, we mainly studied the translation scans at the center and back face of the Tb crystal. Figure 9 shows the translation scans for three different widths of the beam at temperatures below and above T_s. The trapezoid functions drawn in the left-hand panels denote the shape of the beam used for each translation scan on the same scale. The width of the beam measured along the base of the trapezoid is also presented in each figure. The drop in intensity at the back edge of the crystal becomes sharper the narrower beam. The solid curve through the figures on left-hand panels is a calculated curve, scaled to constant intensity in the bulk, obtained by convoluting the beam profile with a step function representing a uniform scattering distribution throughout the crystal. Since the finite scattering angle, albeit very small, relaxes the slope, we have included this effect in the calculation.

The center panels show identical translation scans measured just above T_s at these different beam widths. In these scans, as the beam approaches the crystal c-axis face the intensity does not remain constant. Instead, a truly remarkable enhancement of the intensity is observed, which persists over a limited range of 0.2 K above T_s. As the beam becomes narrower, the enhancement becomes sharper and larger. The solid curves shown in these panels are calculated in the same way as those in the left-hand panels, which correspond to the case where there is no enhancement. As shown in Fig. 10 (obtained from Ref. 8, Fig. 3), the cause of the enhancement becomes apparent by comparing transverse scans at the same temperature at two different translations; one slightly displaced from the crystal face where the enhancement was maximum (6.75 mm) and one at the crystal center (3.50 mm). Slits with a vertical opening of 3 mm (SV) were placed 140 mm after the sample. In addition, a 40′ collimator was placed between SV and the detector. This combination of slits and collimator effectively eliminated the contributions from the top and

bottom faces of the crystal. A wider beam (1.22 mm at the base) was used because of intensity considerations. In both cases the distinctive two-component line shape is present. Whereas the peak intensity of the broad component differs by only 6% in the two scans, that of the narrow component changes by over 70%. The constant background is the same within 4%. Thus, the anomalous enhancement is due to a striking increase in the intensity of the narrow component within the skin of the Tb crystal face, as is obvious from Fig. 10.

Using the calculated curve, scaled to constant intensity in the bulk, we can extract the enhancement at the edge, which is shown in the right-hand panels of Fig. 9. The solid curves in these figures represent the calculated intensity of the narrow component assuming a linear decay after convoluting with the experimentally measured beam shape. In each calculation, the HWHM of the spatial distribution of the scatterer responsible for the narrow component was estimated to be 0.2 mm. It is reasonable to assume that this scatterer is distributed over a finite range because the enhancement always has a width that is considerably larger than that of the neutron beam. That the result of the simulations reproduces the enhancement so well strongly supports this assumption. The details of the calculations mentioned in this section are presented in the Appendix.

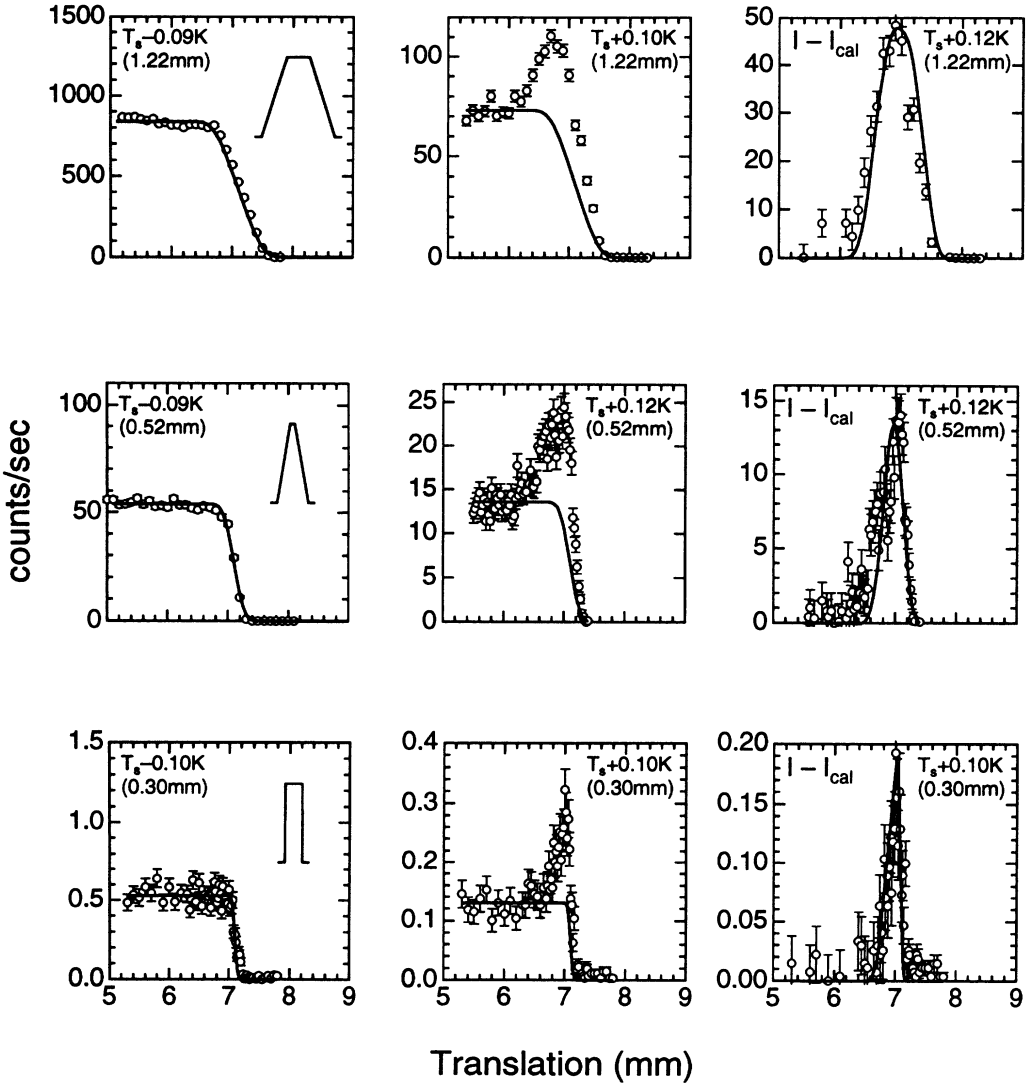

FIG. 9. Translation scans at $(0, 0, \delta)$ below and above T_s at beam widths at the base of 1.22 mm (top), 0.52 mm (middle), and 0.30 mm (bottom) measured on BT7 in NIST. (left) Translation scans below T_s and calculated curves on the basis of a model calculation. (center) Identical scans above T_s showing the enhancement at the c-axis face. (right) Enhancement at the edge extracted by using the calculated curves scaled to constant intensity in the bulk.

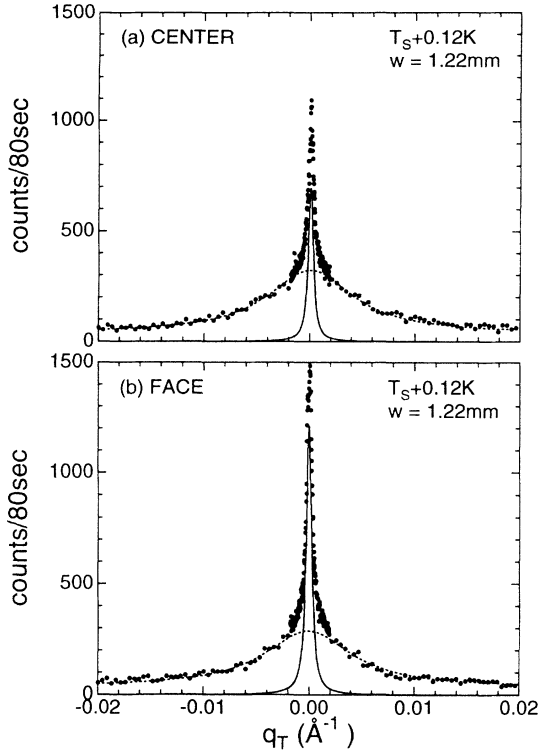

FIG. 10. (a) Transverse-q scan just above T_s at the crystal center (3.50 mm). (b) Identical scan taken at the crystal face (6.75 mm) showing enhanced narrow component. These data were taken at BT7 in NIST. The figures are obtained from Ref. 8, Fig. 3.

VI. QUASISTATIC CHARACTER OF THE NARROW q COMPONENT

As discussed in the preceding sections, the marked difference between the spatial distributions, as well as the temperature dependence of the wave vector δ, of the narrow and broad q components establishes the narrow q component as a distinct entity which contributes to the scattering associated with the critical fluctuations. It is thus natural to expect the energy scale of the narrow q component to differ from that of the broad one. This situation is in contrast to the relationship that exists between the central peak and the soft mode as revealed by energy scans on $SrTiO_3$.[15] In this case, the central peak can be explained by a coupling of the soft mode phonon to a relaxational degree of freedom. Moreover, it has been shown that the broad q component observed in the x-ray studies of $SrTiO_3$ is due to the integrated intensities of the soft mode phonon and the central peak.[4]

The H8 triple-axis spectrometer was used to perform energy scans at $(0,0,\delta)$ in order to examine the energy scales of both the broad and narrow q components. An incident neutron energy E_i of 4.0 meV was used for the most part with a very tight collimation of 10′-10′-sample-10′-10′. At such a small scattering angle, the resolution function is extremely focused in the energy direction as well as in the transverse-q direction. In fact, as shown in Fig. 11(a), an energy scan of the Bragg peak at $T_s - 0.11$ K exhibits a very sharp peak with a full width at half-maximum (FWHM) of only $2\Gamma = 4.0$ μeV, which represents the energy width of the resolution function. The solid curve is a fit to a Lorentzian line shape. Figure 11(b) shows an identical energy scan measured at $T_s + 0.09$ K in which the energy width is considerably larger than that of the Bragg peak. The solid curve is again a fit to a Lorentzian line shape.

In order to analyze the energy scans properly, we must consider not only the Bragg width but also the shape and orientation of the resolution function. The calculated resolution function, projected onto the energy and transverse-q (E-q_T) plane, is shown in Fig. 12(a) along with the FWHM of the narrow q component at $T_s + 0.09$ K. It is clear that, in spite of its extremely narrow energy width, the tilt of the long axis of the resolution ellipsoid in the E-q_T can significantly influence peak profiles under certain scanning conditions. In the energy and longitudinal-q (E-q_L) plane, by contrast, the ellipsoid is not tilted and is in fact nearly circular. As an example, we consider the extreme case where the narrow q component has no energy width. Because the resolution ellipsoid is tilted with respect to the q_T axis, it will intercept the narrow q-component cross section at a finite energy as the ellipsoid is scanned along the energy axis. More importantly, this energy is higher the larger the narrow component q width. Therefore, it is possible that

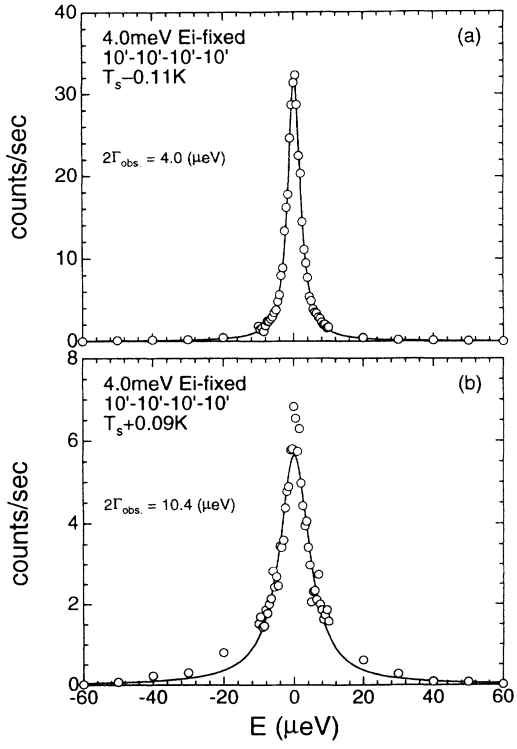

FIG. 11. Energy scans of the $(0,0,\delta)$ peak at (a) $T_s - 0.11$ K and (b) $T_s + 0.09$ K measured on H8 in BNL using $E_i = 4.0$ meV and 10′-10′-S-10′-10′. Curves through the figures are fits to a Lorentzian line shape.

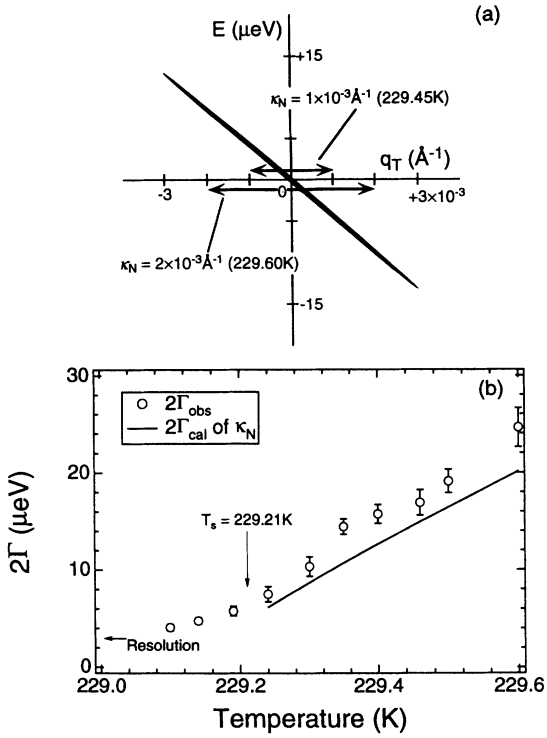

FIG. 12. (a) Projection of the resolution ellipsoid onto the energy and transverse-q plane along with FWHM of the narrow components at 229.45 K and 229.60 K. (b) Temperature dependence of energy width measure on H8 in BNL using E_i = 4.0 meV and 10′-10′-S-10′-10′. Solid line denotes the calculation of the q width appearing in energy scans through the elongated resolution ellipsoid.

temperature-dependent changes in the observed energy linewidth $2\Gamma_N$ of the narrow q component result from corresponding changes in its transverse-q width. Using the observed temperature dependence of the narrow q-component linewidth in the transverse-q direction (see Fig. 7), we can estimate its effect on the energy scans. The solid line in Fig. 12(b) shows the calculated temperature dependence of $2\Gamma_N$ assuming its temperature dependence comes entirely from that of κ_N. The experimentally measured values of $2\Gamma_N$ follow this curve very closely. This result implies that the intrinsic energy width of the narrow q component is essentially temperature independent, and is of order $\sim$2 μeV FWHM, which is extremely small.

Preliminary measurements were carried out in order to characterize the q dependence of the broad component energy width by performing energy scans displaced from the $(0,0,\delta)$ satellite peak by a small amount Δq. Such scans exhibit a considerably larger linewidth $2\Gamma_B$ which increases with increasing Δq. At T_s+0.09 K, for example, $2\Gamma_B$ = 27.7 μeV for Δq = 0.003 Å^{-1} and $2\Gamma_B$ = 47.4 μeV for Δq = 0.006 Å^{-1}. We also observed that the linewidth becomes broader with increasing temperature. Although more extensive studies are required to determine the scattering function precisely, our measurements are consistent with those expected from a standard paramagnetic cross section.

The long axis of the resolution ellipsoid grows quickly with increasing incident neutron energy. The observed Bragg width, however, has a much less severe dependence on incident energy. As mentioned above, the tilt of the long axis of the resolution ellipsoid in the E-q_T plane acts to broaden the observed energy width of any scattering cross section having a finite transverse-q width. Using an incident neutron energy E_i of 14.7 meV with collimation 10′-10′-sample-10′-20′, for example, increases the length of the long axis by a factor of 10. In this configuration, it is actually more difficult to separate the energy width of the narrow component from that of the broad component. Although an energy scan at T_s + 0.12 K taken with E_i = 14.7 meV shows a clear two-component line shape similar to that seen in transverse-q scans, such a clear-cut two-component profile is deceptive because the energy-broadening effect of the finite q width becomes more pronounced at higher E_i. The finite q widths of both the narrow and broad q components are being projected into the energy scan as a result of the tilt of the highly elongated resolution function. Therefore, in order to measure the energy profiles of the two components accurately, it is best to use a small enough incident neutron energy to avoid the energy broadening induced by the finite q width.

Summarizing briefly, our experimental results indicate that the broad q component has a small but finite energy width of several 10 μeV, which becomes broader with increasing Δq and temperature. The energy width of the narrow q component, however, is indistinguishable from the elastic scattering within our resolution. The narrow q component exhibits a quasi-Bragg peak with a temperature-dependent q width.

VII. DISCUSSION

The combination of translation and transverse-q scans presented in Figs. 9 and 10, respectively, demonstrate that the the narrow q component originates in the near-surface volume or "skin" of the Tb crystal. A detailed analysis of the translation scans shows that the skin thickness is about 0.2 mm, which is enormous compared to typical surface effects. Using this knowledge, we can reinterpret previous experimental results obtained from studies of $SrTiO_3$, Ho, and other compounds. In his x-ray-scattering measurements on $SrTiO_3$, for example, Andrews[1] pointed out that the ratio of surface to bulk scattering intensities did not appear to depend on the x-ray penetration depth, a result which was hard to understand in terms of a surface layer model but which would be expected if the observed critical behavior originated in the the crystal bulk. However, we believe that it is more likely that the narrow q component of $SrTiO_3$ is also highly concentrated in the skin. This does not necessarily contradict Andrew's statement because the narrow q component can be spread over several tens or hundreds of μm, which is much deeper than typical x-ray penetration depths. A series of more recent experiments on $SrTiO_3$ reported that only the broad q component is seen in neutron-scattering measurements,[4,16] whereas

x-ray-scattering measurements show both components. Thus, if the skin in $SrTiO_3$ is too thin to provide a sufficient neutron-scattering intensity, this paradox can be rationally explained. Thurston *et al.* mentioned essentially the same experimental results in their x-ray- and neutron-scattering studies on Ho.[5]

There are several important questions regarding the spatial distribution of the narrow q component which remain unanswered. One is whether or not an anisotropy of the narrow q-component skin thickness or population exists between the c-axis face and the orthogonal faces. Such an anisotropy seems quite plausible in view of the fact that all the spins lie within the basal c-axis plane in the spiral phase of Tb. We have realized that the use of vertically collimating slits in both translation and transverse-q scans give enough information to solve this problem, and our preliminary measurements support the presence of such an anisotropy. A second problem is whether or not the narrow q component vanishes in the bulk, and whether or not the broad q component is depleted at the expense of the narrow q component in the skin. In principle, it is possible to isolate the scattering from the bulk from that due to the skin by placing sufficiently narrow slits in both the incident and scattered neutron beams. This technique was employed by Cowley and Shirane in 1978 on a single crystal of $SrTiO_3$.[17] However, in order to apply this technique to Tb, a much larger crystal is needed because the scattering angle at $(0,0,\delta)$ is very small. To eliminate completely the scattering from the four crystal faces orthogonal to the c-axis face would, given the 7 mm thickness of our Tb crystal, require a slit so narrow that experimental counting times would be prohibitive. Therefore, because a wider slit had to be used, the narrow q component inevitably appears in all transverse-q scans no matter what crystal translation setting is used. We are in process of setting up a new experiment using a much larger crystal in an effort to isolate the true bulk scattering using this technique.

We have established two very important results concerning the nature of the narrow q component that yield significant insight into the microscopic origin of the second length scale. We have shown that the spatial distribution of the narrow q component is sharply peaked within a 0.2 mm thick region of the crystal surface, a marked contrast to the essentially uniform distribution of the broad q component. In addition, we have shown that the narrow q component possesses a different temperature dependence of the wave vector δ and a distinct, quasistatic energy scale. These results indicate that quasistatic clusters, which are considerably larger than the usual fluctuating regions, are formed in the crystal skin above T_s. It is possible that these clusters have their own intrinsic T_s, which is higher than the bulk T_s. We have actually tried to measure the depth dependence of T_s by performing transverse q scans at a finite energy transfer on H8 using a narrow neutron beam. As a result, identical values of T_s were observed in both the skin and bulk. However, we now realize that this technique only measures the T_s of the broad q component in either the skin or in the bulk. Until now, we have not been able to develop a technique which can measure the T_s of the narrow q component.

We speculate that an inherent relation exists between the narrow and broad q components. Intuitively, we assume that the narrow q component develops only when the broad q-component correlation length grows sufficiently large. This is exactly what happens in the case of the central peak in $SrTiO_3$; the central peak appears and diverges only after the soft mode gets soft enough.[15] We have experimentally determined that, over the temperature range where the two-component line shape is observed, the intensities of the narrow q component $I_N(T)$ and the broad q component $I_B(T)$ follow the simple relation $I_N(T) \propto I_B(T)^{4.0}$. The exponent in this relation may be sample dependent. A similar but quadratic relation has been found to hold between the central peak and the soft mode phonon intensities in $SrTiO_3$.[4]

At present, no theory provides a complete explanation of the results obtained in the current study. We briefly summarize several models which describe the spatial correlations above the transition temperature, and which have been quoted often in previous studies of the two-length-scale phenomena. In order to obtain an understanding of their x-ray-scattering results on $RbCaF_3$,[6] Ryan *et al.* referred to a model proposed by Imry and Wortis[18] in 1979 involving defect-induced fluctuations that arise from parts of the crystal fluctuating between different free-energy minimums. These fluctuations have a longer correlation length than that of the usual small fluctuations about the local minimum of the free-energy function for each phase, which account for the broad q component of the critical scattering. This theory is, however, specific to first-order transitions and does not require an inhomogeneous distribution of defects. Osterman *et al.* invoked inhomogeneous surface strains that couple quadratically to the order parameter, thus renormalizing T_c, to explain a dependence of the superlattice reflection intensity in $SrTiO_3$ on x-ray penetration depth.[19] Under such conditions, the surface can order before the bulk with a new characteristic length scale.[20] Recently, Axe has proposed extending this idea of quadratic strain-order parameter coupling to more general inhomogeneous strain distributions. It appears that a quasistatic second length scale giving rise to scattering with Lorentzian-squared q dependence can arise naturally in such a model.[21] These features are in a good agreement with the results obtained in the current study of Tb. It is worthwhile to note that strains due to a large magnetostriction in Ho or Tb are enhanced near the surface of the crystal. Thus, as shown in the preceding sections, one can reasonably expect a greater population of the narrow q component in the skin than in the bulk. We await further development of this interesting idea.

ACKNOWLEDGMENTS

We would like to thank J. D. Axe for many stimulating discussions, which often suggested the next experimental step. We have also benefited from discussions with R. A. Cowley, Doon Gibbs, J. P. Hill, and S. M. Shapiro. Work at Brookhaven National Laboratory was supported

by the U.S. Department of Energy, under Contract No. DE-AC02-76CH00016 and by the U.S.-Japan Cooperative Neutron Scattering Program.

APPENDIX: CALCULATION OF THE SKIN THICKNESS

We assume that the narrow q component originates at the crystal surface, but persists to a depth of several hundred μm beneath the surface, whereas the broad q component exists in the bulk phase. For convenience of analysis, we separate the crystal into three parts: (I) the skin of the c-axis face (C skin), (II) the skin of those faces orthogonal to the c-axis face (A and B skins), and (III) the crystal bulk, as shown in Figs. 13(a)–(b). We will use the following notation: The skin thickness is denoted by ϵ, the beam full width is w, the width of the crystal is d (=7.1 mm), and the scattering angle is θ (=1.35°). Note that, as shown in Fig. 13(a), we cannot treat the incident beam as being parallel to the c-axis face, even though θ is very small. This is because a "shadow" appears on the c-axis face, which varies as $d\tan\theta$ (=0.17 mm), which is roughly the same size as the skin thickness ϵ. This shadow broadens the translation scan precisely in the region where the narrow q component exists.

Although it is possible to perform calculations assuming finite widths for both the skin and neutron beam, it is far more convenient and instructive to start with the idealized situation of a narrow skin and a narrow beam. We assume here that the beam width w and the skin thickness ϵ are much smaller than the size of the crystal d. Since the total diffraction intensity I from the skin depends on the area of the beam, each of the A and B skins contributes $I_A \approx \epsilon w/\cos\theta$, while the C skin contributes $I_C \approx \epsilon w/\sin\theta$ [see Fig. 13(b)]. Figures 13(c)–(e) show model translation scans for both the C and $A+B$ skins, and the bulk under these ideal conditions, respectively. R denotes the intensity ratio I_A/I_C.

We can generate a model to simulate the results from our actual experimental setup using the results of the ideal case. First we calculate the scattering contribution from the C skin of the crystal. It is clear that the spatial distribution of the narrow q-component intensity has a depth dependence, and that it decays in some fashion with distance from the crystal surface. At this stage, it is simplest to assume that this decay is linear. In order to make use of the results from ideal case, we divide both the skin and beam into small segments or strips as shown in Fig. 13(f). Integrating along the skin-depth and the beam-width directions while taking into account the spatial distribution of the narrow q component and the beam

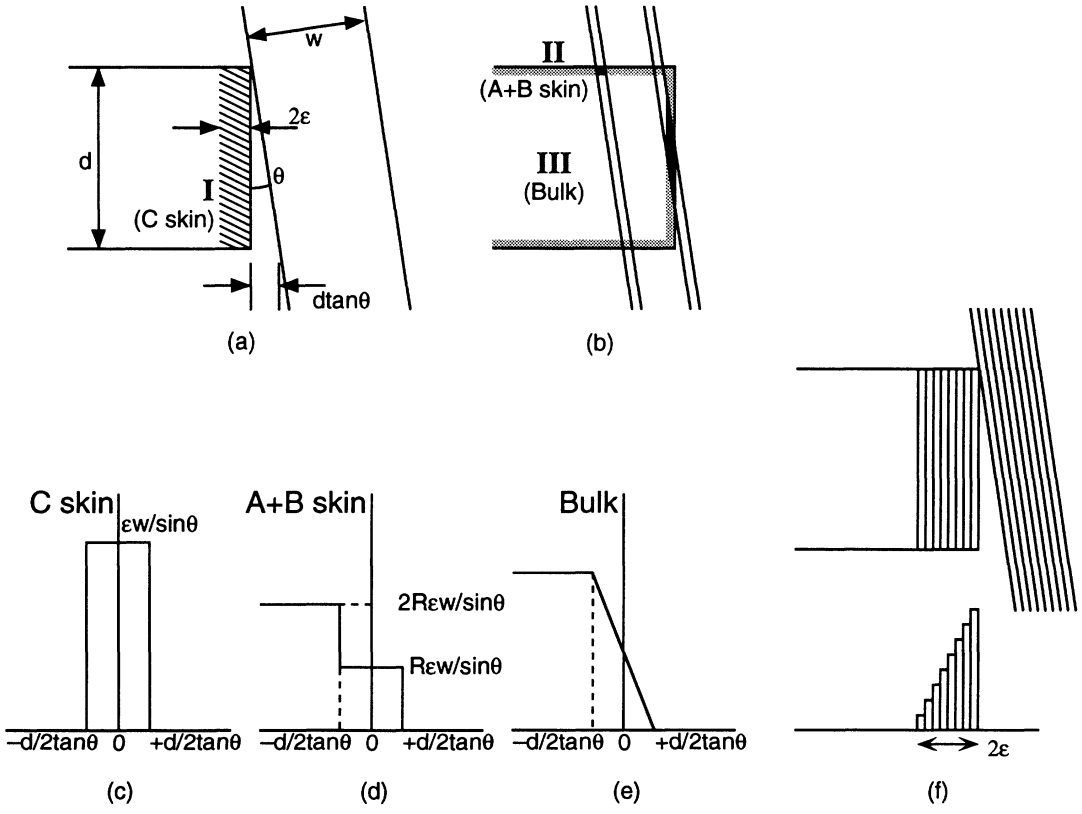

FIG. 13. (a) Schematic diagram of the experimental condition, showing the Tb crystal (size d and the skin thickness ϵ FWHM) and a neutron beam (width w). (b) Schematic diagram of the ideal condition (narrow-skin and narrow-beam regimes). (c) Ideal translation scan of the C skin phase. (d) Ideal translation scan of the A and B skin phases. (e) Ideal translation scan of the bulk phase. (f) Strips of the skin and the beam for a model calculation using the results of the ideal case.

gives us the translation scan through the C skin. This method can be directly applied to a more complicated distribution of the narrow q component. Next, we consider the contributions from the $A+B$ skin and the crystal bulk. In the narrow-skin and narrow-beam regime, these two regions were found to give very different translation scan profiles. However, after integrating as we did for the C skin, we find no significant difference in the translation scan profiles between the bulk and $A+B$ skin regions under our experimental conditions. This is because the shadow effect which results from the finite scattering angle blurs the steep changes at the c-axis face in the translation scans. Therefore, it is not necessary to distinguish them in this model calculation. If we knew the factor R, which measures the anisotropy between the C and A/B skins, then we could separate the translation scan profile of the $A+B$ skin from that of the bulk.

In order to fit our data to the model calculation, we let ϵ and R be adjustable parameters, after scaling the constant part of the translation scan to the experimentally measured value. Thus, the curves in the translation scans below T_s (left-hand panels of Fig. 9) include essentially no adjustable parameters. As shown in Fig. 9, each fit to the translation scans at $T_s + 0.1$ K using different beam widths gives very good and consistent results; the ratio R is 10 ± 2 and the skin thickness ϵ is 0.2 ± 0.05 mm.

[1] S. R. Andrews, J. Phys. C **19**, 3712 (1986).
[2] R. J. Nelmes, P. E. Hatton, and H. Vass, Phys. Rev. Lett. **60**, 2172 (1988).
[3] D. F. McMorrow, N. Hamaya, S. Shimomura, Y. Fujii, S. Kishimoto, and H. Iwasaki, Solid State Commun. **76**, 443 (1990).
[4] G. Shirane, R. A. Cowley, M. Matsuda, and S. M. Shapiro, Phys. Rev. B **48**, 15595 (1993).
[5] T. R. Thurston, G. Helgensen, D. Gibbs, J. P. Hill, B. D. Gaulin, and G. Shirane, Phys. Rev. Lett. **70**, 3151 (1993).
[6] T. W. Ryan, R. J. Nelmes, R. A. Cowley, and A. Gibaud, Phys. Rev. Lett. **56**, 2704 (1986).
[7] U. J. Nicholls and R. A. Cowley, J. Phys. C **20**, 3417 (1987).
[8] P. M. Gehring, K. Hirota, C. F. Majkrzak, and G. Shirane, Phys. Rev. Lett. **71**, 1087 (1993).
[9] C. F. Majkrzak, Physica B **173**, 75 (1991).
[10] W. C. Koehler, J. W. Cable, E. O. Wollan, and M. K. Wilkinson, J. Phys. Soc. Jpn. **17**, Suppl. B-III, 32 (1962); W. C. Koehler, J. Appl. Phys. **36**, 1078 (1965).
[11] P. M. Gehring, L. Rebelsky, D. Gibbs, and G. Shirane, Phys. Rev. B **45**, 243 (1992).
[12] N. J. Chesser and J. D. Axe, Acta Crystallogr. A **29**, 160 (1973).
[13] F. J. Darnell, Phys. Rev. **132**, 1098 (1963).
[14] Franco Jona and G. Shirane, *Ferroelectric Crystals* (Pergamon Press, Oxford, 1962).
[15] S. M. Shapiro, J. D. Axe, G. Shirane, and T. Riste, Phys. Rev. B **11** 4332 (1972).
[16] K. Hirota, J. P. Hill, Y. Fujii, S. M. Shapiro, and G. Shirane (unpublished).
[17] R. A. Cowley and G. Shirane, J. Phys. C **11** L939 (1978).
[18] Y. Imry and M. Wortis, Phys. Rev. B **19**, 3580 (1979).
[19] D. P. Osterman, K. Mohanty, and J. D. Axe, J. Phys. C **21** 2635 (1988).
[20] T. C. Lubensky and M. H. Rubin, Phys. Rev. B **12**, 3885 (1975).
[21] J. D. Axe (private communication).

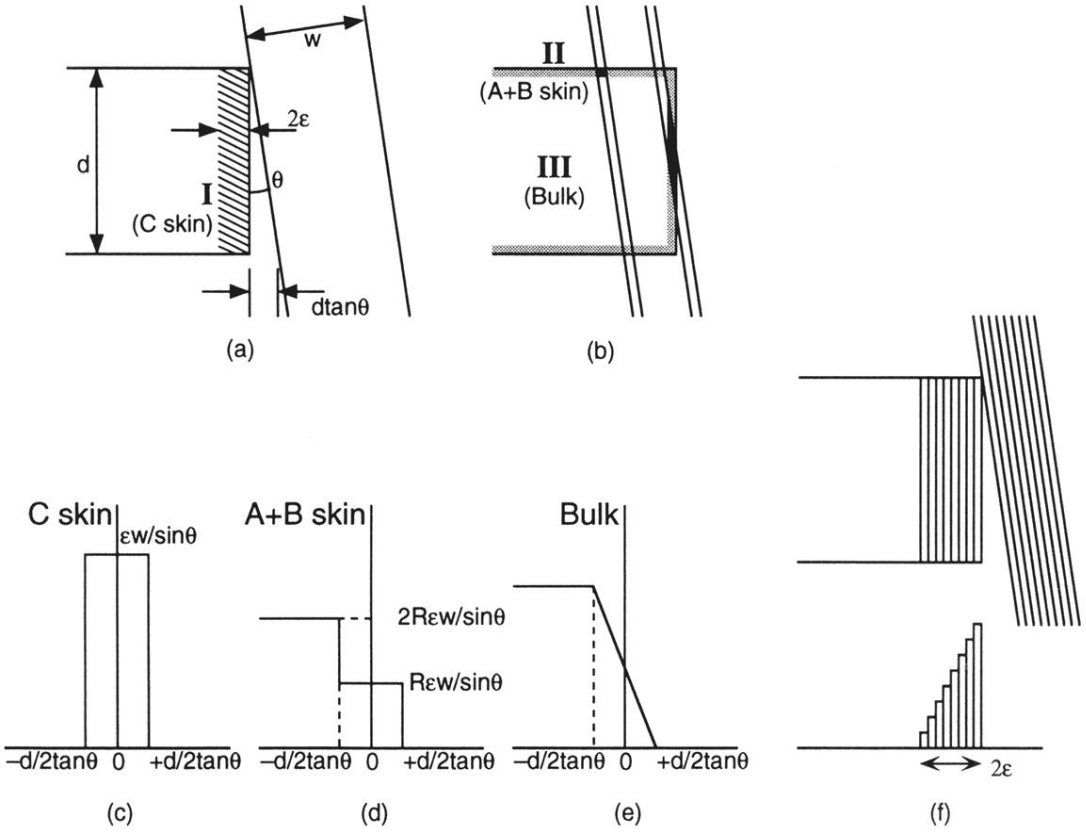

FIG. 13. (a) Schematic diagram of the experimental condition, showing the Tb crystal (size d and the skin thickness ϵ FWHM) and a neutron beam (width w). (b) Schematic diagram of the ideal condition (narrow-skin and narrow-beam regimes). (c) Ideal translation scan of the C skin phase. (d) Ideal translation scan of the A and B skin phases. (e) Ideal translation scan of the bulk phase. (f) Strips of the skin and the beam for a model calculation using the results of the ideal case.

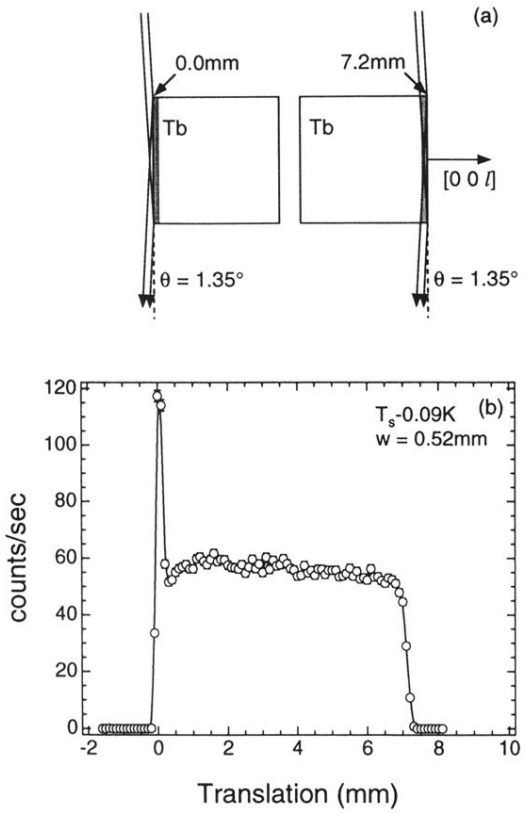

FIG. 8. (a) Schematic diagram of scattering geometry. (b) Translation scans at $(0, 0, \delta)$ below T_s at beam width at the base of 0.52 mm measured on BT7 in NIST.